iScience

CellPress
OPEN ACCESS

Article

First-principles study of MXene properties with varying hydrofluoric acid concentration

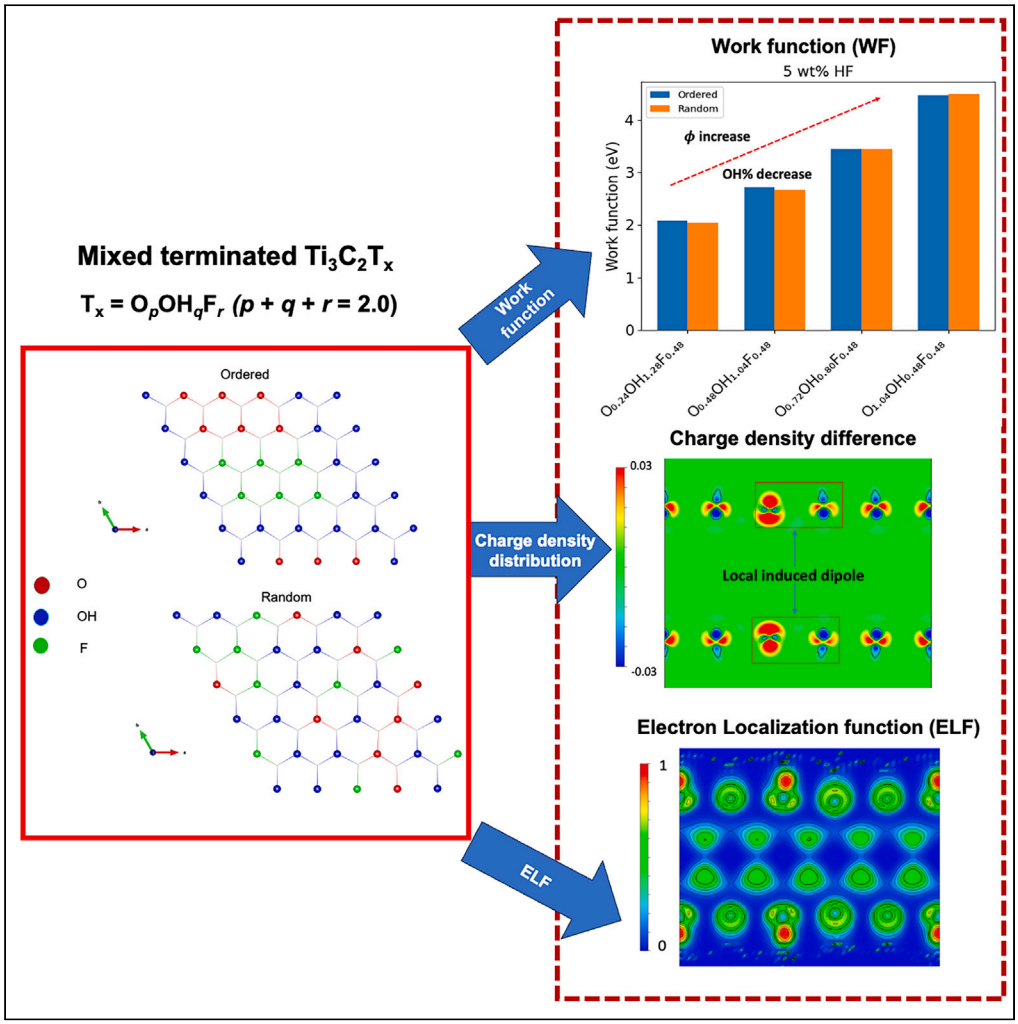

Yi Zhi Chu, Megan Hoover, Patrick Ward, Kah Chun Lau

kahchun.lau@csun.edu

Highlights

Ordered and random ternary mixed terminated Ti_3C_2 surfaces are studied

Hydroxyl group (-OH) plays a pivotal role in the surface's electronic properties

Locally induced dipoles on the surface render favorable reaction sites

Chu et al., iScience 27, 108784
February 16, 2024
https://doi.org/10.1016/j.isci.2024.108784

iScience

CellPress
OPEN ACCESS

Article

First-principles study of MXene properties with varying hydrofluoric acid concentration

Yi Zhi Chu,[1,4] Megan Hoover,[2] Patrick Ward,[3] and Kah Chun Lau[4,5,*]

SUMMARY

With varying hydrofluoric acid (HF) concentrations under three etching conditions, we presented a comparative study of the effects of both the ordered and randomly ternary mixed terminated $Ti_3C_2T_x$ surfaces with a wide variation of O/OH/F stoichiometry on the thermodynamic stability and electronic properties. Regardless of the HF concentration, an OH-rich surface is found to be thermodynamically stable and the electrical conductivity of $Ti_3C_2T_x$ is substantially affected by the OH concentration. The charge density difference and electron localization function demonstrated a significant electron localization at the hydroxyl group on the O/OH/F mixed terminated surface, which could yield a locally induced dipole on the surface that renders favorable reaction sites on the functionalized surface. In addition, a large tunability in the work function ($\Delta\Phi \sim 3.5$ eV) is predicted for $Ti_3C_2T_x$. These findings provide a pathway for strategically tuning the electronic and structural properties of Ti_3C_2 MXenes etched with HF.

INTRODUCTION

The active research of two-dimensional (2D) materials conducted since the successful exfoliation of graphene[1] in 2004 has led to the discovery of a new, emerging class of 2D materials consisting of carbides and nitrides of transition metals, known as MXenes.[2] MXenes are two-dimensional materials with the general formula $M_{n+1}X_nT_x$, where M is an early transition metal (e.g., Ti, V, and Cr), X is carbon, nitrogen or carbonitride, and T is the surface termination group composed of O, OH, F, and/or Cl.[2] Due to their compelling physical, electronic, and chemical properties, MXenes have attracted immense theoretical and experimental research interests in a variety of applications, such as Li-ion batteries,[3,4] gas sensors,[5] hydrogen storage,[6] and thermoelectrics.[7] Among those studies, nearly 70% have been devoted to $Ti_3C_2T_x$, the first ever experimentally synthesized MXene.[8] It is considered the most comprehensively studied MXene to date.

$Ti_3C_2T_x$ can be selectively etched from its MAX phase with hydrofluoric acid (HF), where A is an A group element typically from groups 13 and 14 of the periodic table (A = Al for $Ti_3C_2T_x$).[8] Due to the highly reactive Ti surface after etching, the exfoliated $Ti_3C_2T_x$ often consists of randomly distributed surface functional groups (i.e., O, OH, and F), which are collectively expressed as T_x.[9] However, due to the complexity and computational cost of simulating mixed terminated surfaces, most of the theoretical studies have considered either the bare Ti_3C_2[10,11] or the uniformly terminated $Ti_3C_2T_x$ with a single functional group.[4,7,12–14] This is often regarded as the first- and second-generation model of MXenes.[15] Early experimental efforts such as powder X-ray diffraction (XRD),[8] high-resolution transmission electron microscopy (TEM),[8,9,16] and X-ray atomic pair distribution function (PDF)[17] were used to gain insight into the distribution of the functional group compositions. However, each method was hindered by its insensitivity to hydrogen, which is essential for understanding the surface termination.[15] Thus, using the atomic PDF supported by a high-quality neutron total scattering method, Wang et al.[15] obtained the first resolution of the $Ti_3C_2T_x$ structure synthesized under different conditions and proposed a multilayered structural model of $Ti_3C_2T_x$ to be the next-generation model of MXenes.

Inspired by the work from Wang et al., several theoretical investigations focused on the effect of mixed functional group terminations (O, OH, and F). Caffrey[18] proposed an empirical model to study the change in the structural and electrochemical properties of the mixed terminated $Ti_3C_2T_x$ and V_2CT_x structures compared to that of the uniformly terminated surfaces. According to the Caffrey study, the empirical model reproduces the lattice parameter, electron density of states (eDOS), and work function that are consistent with experimental data. To date, the most comprehensive study on the distribution and composition of the surface functionalization of 2D MXenes employing the cluster expansion method was conducted by Ibragimova et al.[19] In that study, the optimum O:OH:F composition was 50:25:25 under standard hydrogen electrode (SHE) conditions, with similar distribution patterns that were unaffected by thickness and type of MXene.

Nevertheless, the design pathway for tuning the mixed surface termination is still absent from the literature. Using energy dispersive X-ray spectroscopy (EDX) in the PDF characterization, Wang et al.[15] estimated the average atomic ratio of O:F in the multilayer $Ti_3C_2T_x$ sample to be 0.85 and 1.4 when etched with 48 wt. % and 10 wt. % HF, respectively. Based on those O:F ratios, Wang et al. derived the stoichiometry of

[1]Department of Physics, Michigan Technological University, Houghton, MI 49931, USA
[2]Advanced Modeling and Simulations, Savannah River National Laboratory, Aiken, SC 29803, USA
[3]Materials Technology and Energy Division, Savannah River National Laboratory, Aiken, SC 29803, USA
[4]Department of Physics and Astronomy, California State University, Northridge, CA 91330, USA
[5]Lead contact
*Correspondence: kahchun.lau@csun.edu
https://doi.org/10.1016/j.isci.2024.108784

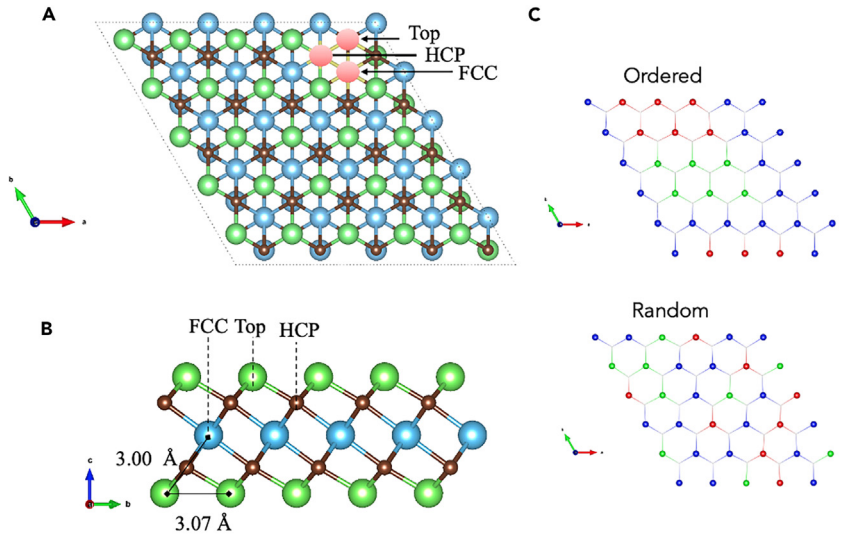

(A) Top view of the $Ti_3C_2T_x$ crystal structure, where green: Top Ti, blue: Middle Ti, brown: C.
(B) Side view of the crystal structure of $Ti_3C_2T_x$, where green: Top Ti, blue: Middle Ti, brown: C.
(C) The demonstration of an ordered and random distribution of surface functional group adatoms, where red: O, green: F, blue: OH.

Figure 1. $Ti_3C_2T_x$ crystal structure

(A) Top view of the $Ti_3C_2T_x$ crystal structure, where green: Top Ti, blue: Middle Ti, brown: C.
(B) Side view of the crystal structure of $Ti_3C_2T_x$,where green: Top Ti, blue: Middle Ti, brown: C.
(C) The demonstration of an ordered and random distribution of surface functional group adatoms, where red: O, green: F, blue: OH.

T_x, which is equal to $O_{0.1}(OH)_{0.8}F_{1.1}$ and $O_{0.13}(OH)_{1.04}F_{0.83}$. In addition, the overall crystallinity and ordering are also affected by the concentration of HF. A higher concentration of HF yields higher F composition in the surface termination. Intuitively, this is consistent with an increased probability of F being available to terminate the freshly etched surface of Ti with higher HF concentrations. Hence, inspired by the findings from the Wang et al. and the cluster expansion studies,[19] the thermodynamic stability and electronic properties of $Ti_3C_2T_x$ with different surface terminations were investigated.

RESULTS AND DISCUSSION

Formation energy and thermodynamic stability

As a benchmark for comparison with the O-, OH-, F-mixed terminated surfaces, a single-layer $Ti_3C_2T_x$ sheet uniformly terminated with the O, OH, and F functional groups (i.e., $Ti_3C_2T_x$, where T_x is represented by $O_pOH_qF_r$ and $p+q+r = 2.0$), is considered. A 5 × 5×1 supercell of Ti_3C_2 was constructed, where both surfaces were populated with the functional group adatoms (Figure 1), corresponding to a total of 25 adsorption sites per surface. For a pristine 2D Ti_3C_2 surface, there are three possible high-symmetry adsorption sites for the adatoms, namely top (on top of the outer layer Ti atoms), face centered cubic (FCC) (on top of the middle layer Ti atoms in the hollow site), and hexagonal close packed (HCP) (on top of the C atoms in the hollow site) as shown in Figures 1A and 1B. The formation energies are calculated as $E_{formation/adatom} = (E_{Ti_3C_2T_x} - E_{Ti_3C_2} - nE_{T_x})/n$, where $E_{formation/adatom}$, $E_{Ti_3C_2T_x}$, $E_{Ti_3C_2}$ and E_{T_x} are the formation energy (per adatom), total energy of $Ti_3C_2T_x$, total energy of the bare Ti_3C_2 structure, and the energy of the functional group adatoms in the gas phase. The number of adsorbed adatoms is denoted by n.

From the reported literature,[4,7,10–14] most of the previous theoretical studies on a homogeneous or mixed-surface termination focused solely on a fully terminated surface. In addition, they have found that the FCC site is the most favorable adsorption site for the full termination of O/OH/F single species. Complementary to these prior studies,[4,7,10–13] a basic understanding of the change in the thermodynamic stability transitioning from the bare Ti_3C_2 structure to fully terminated $Ti_3C_2T_x$ structure provides valuable insight into the influential factors of surface termination. By gradually increasing the percent coverage of adatoms on the bare Ti_3C_2 surface the thermodynamic stability of $Ti_3C_2T_x$ can be systematically evaluated. The preferred binding sites for different single-adatom coverages can aid in constructing the mixed terminated $Ti_3C_2T_x$ surface. Among all the $Ti_3C_2T_x$ distributions considered at different percentage coverages, the adatoms preferred the FCC sites, regardless of the percent coverage on the Ti_3C_2 surface.

In this study, an ordered and random distribution is considered when terminating the Ti_3C_2 surface, wherein the surface adatoms are distributed in an orderly manner such that each O, OH, and F termination species is located close to each other forming a cluster-like region for the ordered distribution. This is in contrast to the randomly distributed adatoms for the random distribution (Figure 1C). The random model was constructed by assigning the FCC sites adatoms and performing structural optimization. The details of the model construction

Table 1. Formation energy of various mixed terminated $Ti_3C_2T_x$ structures with two different local site distribution of O/OH/F adatoms (i.e., ordered vs. random)

		Formation energy/adatom (eV/adatom)	
System	T_x stoichiometry	Ordered	Random
O:F = 0.8	$O_{0.24}OH_{0.64}F_{1.12}$	−5.46	−5.47
48 wt. % HF	$O_{0.40}OH_{0.48}F_{1.12}$	−5.37	−5.39
	$O_{0.64}OH_{0.24}F_{1.12}$	−5.23	−5.25
	$O_{0.80}OH_{0.08}F_{1.12}$	−5.12	−5.14
O:F = 1.3	$O_{0.24}OH_{0.88}F_{0.88}$	−5.54	−5.55
10 wt. % HF	$O_{0.48}OH_{0.64}F_{0.88}$	−5.41	−5.43
	$O_{0.64}OH_{0.48}F_{0.88}$	−5.32	−5.34
	$O_{0.88}OH_{0.24}F_{0.88}$	−5.17	−5.19
O:F = 3.2	$O_{0.24}OH_{1.28}F_{0.48}$	−5.65	−5.66
5 wt. % HF	$O_{0.48}OH_{1.04}F_{0.48}$	−5.53	−5.57
	$O_{0.72}OH_{0.80}F_{0.48}$	−5.40	−5.45
	$O_{1.04}OH_{0.48}F_{0.48}$	−5.20	−5.22

The O:F ratio corresponds to different HF concentrations according to ref. 15.
Thermal energy corrections are included in the calculation of the energy values in Table 1. As comparison, another reference energy model considering the experimental conditions following the Ref. [19,20] (including thermal energy corrections) is included in Table S1.

can be found in the supplemental information. The surface distributions presented here are the representative cases with the lowest energy for each stoichiometry.

Table 1 shows the formation energy of various surface terminations under three different etching conditions. The atomic ratio O:F corresponds to the concentration of HF during etching, representing 48 and 10 wt. % for O:F = 0.85 and 1.4, respectively (as adapted from Wang et al.[15]). Employing the same terminology, the O:F ratio that mimics a weak acidic environment (~5 wt. % HF), is derived from the stoichiometry of $T_x = O_{1.04}(OH)_{0.48}F_{0.48}$. Due to the limitation of the simulation cell, the O:F ratios considered in this work are 0.8, 1.3, and 3.2 for 48, 10, and 5 wt. % HF, respectively.

In previous work,[15] the O:F ratio was obtained by considering all oxygen atoms present in $Ti_3C_2T_x$, including those associated with the hydroxyl group (OH). In addition, the OH fraction was explicitly set as a constant in the derivation of the T_x stoichiometry. In this work, to study the effect of varying the OH fraction, the F fraction is fixed, while the O and OH fractions are varied. This results in two different surface coverages: OH fraction that is either higher (OH-rich) or lower (OH-poor) than the O fraction (Table 1).

From density functional theory (DFT) calculations, the $Ti_3C_2T_x$ stability is more sensitive to the relative stoichiometry of O, OH, and F adatoms on the surface rather than the local site distribution of adatoms (Table 1). Using gas phase O_2/F_2 and isolated OH as the reference energy, our calculations show a decreasing trend in the formation energy as the OH fraction decreases. As shown in Table 1, the OH-rich coverages are thermodynamically stable, regardless of the HF concentration. Furthermore, the ordered and random terminated structures are found to be degenerate in terms of formation energy (Table 1). Both the ordered and random distribution of O/OH/F adatoms (Figure 1C) exhibit nearly similar thermodynamic stability, where the structures with random distribution are ~0.01–0.04 eV more stable than that of the ordered distribution (Table 1).

Based on the thermodynamic stability study of the partially terminated surfaces, local clustering of O adatoms tends to be less stable (~0.2–0.3 eV/adatom), especially for the lower coverages (i.e., ≤60%). This trend is less profound in partial surface termination with local clustering of OH and F adatoms, especially for F adatoms (Figure S1). Hence, the difference in the formation energy between the ordered and random distribution is determined by local O-clustering especially at low concentrations, as seen in the nearest neighbor analysis (see Figures S5–S10). The O-O fraction is predominantly the first nearest neighbor in the ordered distribution instead of the second and third nearest neighbors, implying a signature of local clustering of O adatoms could be a factor in distinguishing an ordered from a random distribution.

Based on the partial termination study, we have found an empirical relationship to predict the relative stability between the structures. The O adatom has a stronger effect on the overall stability of $Ti_3C_2T_x$, with an energy difference of ~0.6 eV/adatom between the bare and full termination surfaces, followed by OH with a ~0.2 eV/adatom difference. In contrast, F adatoms do not significantly vary the thermodynamic stability of the structure, where nearly a constant of −5.3 eV/adatom formation energy is observed when transitioning from the bare to full F-terminated surface. This could explain the subtle difference in formation energy (~0.2 - ~0.3 eV) between the structures etched with different wt. % HF, as the thermodynamic stability is insensitive to the variation of F concentration, but mostly determined by the relative content of O and OH adatoms.

Due to the fact that MXene surface is highly tunable with a variation possibility on the M, X, and T_x positions, therefore multiple factors can be readily tuned in MXenes surface chemistry. Our partial termination study (shown in Figure S1) also demonstrated the importance of local clustering of O/OH/F species, which motivates the construction of local ordered distribution in surface termination. In Figure S1, it is found that for partial F termination, the ordered and random surface termination is energetically degenerate. For OH termination, a subtle energy

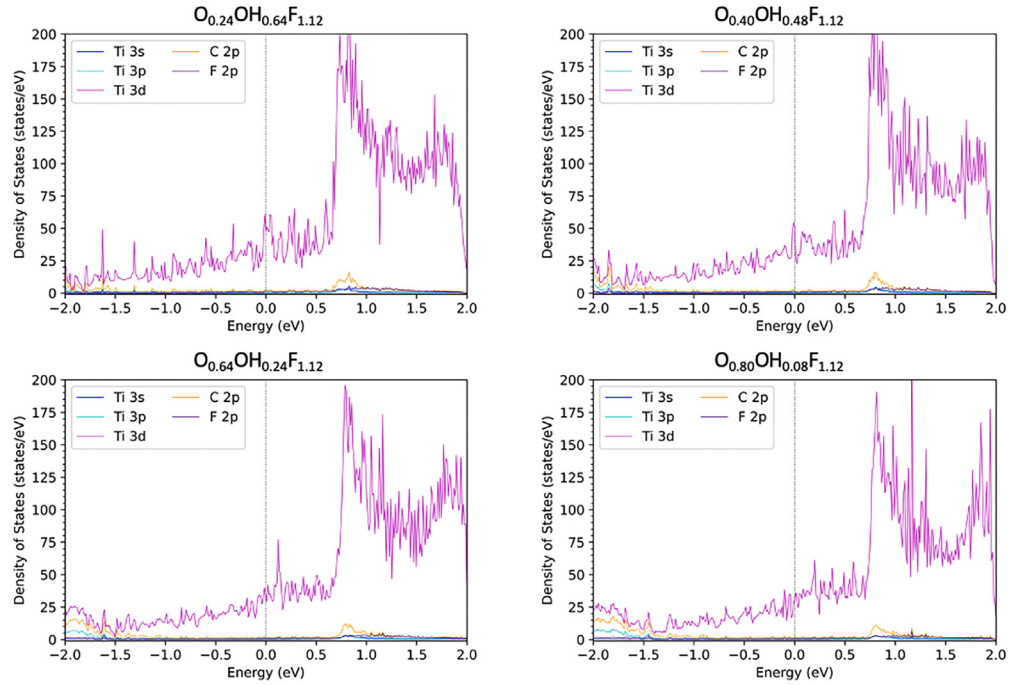

The Fermi level, E_F is set to zero.

Figure 2. Electron density of states of $Ti_3C_2T_x$ etched with 48 wt. % HF

The Fermi level, E_F is set to zero.

difference of less than 0.05 eV/adatom between the ordered and distribution is observed when OH percent coverage is increased, indicating competitive stability between the two types of distributions. While the O termination exhibits a slightly different trend where a local clustering of O at lower percent coverage is less favorable, whereas at higher percent coverage (framed in red), the energy difference between ordered and random surface termination is less than ~0.10 eV/adatom. This observation highlights the importance of studying the different types of surface distributions of termination groups, besides the variation in mixed stoichiometry of surface termination.

Electronic properties

Electron density of states (eDOS)

To identify the general features of the electronic structure among different O/OH/F terminations on the $Ti_3C_2T_x$ structure, the eDOS is calculated in an energy range near the Fermi level, E_F. Overall, the metallic nature of $Ti_3C_2T_x$ is evident due to the presence of finite electronic states at Fermi level (E_F) regardless of the terminating adatoms and their distribution. From Figure 2, the Ti *3d* orbital dominates the electronic states throughout the energy range from −0.5 to 0.5 eV within the vicinity of E_F in all cases. This indicates that the 3d orbital would contribute the most to the tunneling current in STM characterization. The eDOS at E_F, i.e., N(E_F) of all structures is within the range of ~30–~50 states/eV (see Figures S3 and S4). Wang et al.[21] studied the surface properties of $Ti_3C_2T_x$ and observed the tunable conductivity with different surface termination species. With uniform termination species, OH termination has the highest electronic states at E_F. Our calculation shows a consistent observation where the N(E_F) of a uniformly O-terminated surface is the highest compared to that of an O/F-terminated surface.

Figure 2 shows the partial density of states (pDOS) of $Ti_3C_2T_x$ with ordered surface distribution etched with 48 wt. % HF. Interestingly, $Ti_3C_2T_x$ OH-rich surfaces consist of a larger magnitude of eDOS at E_F, (N(E_F) ~50 states/eV) than that of OH-poor surfaces (N(E_F) ~30 states/eV). Similar results were observed for randomly terminated surfaces. While there are no clear empirical relationships between the O/OH/F concentrations and N(E_F), it is noted that in general, the surface with excess OH concentration has an upper limit of N(E_F) saturated at ~50 states/eV, compared to the lower limit of N(E_F) around ~30 states/eV with excess O concentration. Thus, lower electronic conductivity is expected for surfaces with lower OH concentration. Of note, the N(E_F) of the uniformly OH-terminated Ti_3C_2 surface is nearly twice (~90 states/eV) as much as the uniformly F-/O-terminated surfaces (see Figure S2). However, when the mixed terminated O/OH/F surface is present, the N(E_F) is substantially suppressed to fall within the range closer to that of the F-/O-terminated surface (*i.e.*, ~40 states/eV). Thus, we believe the increase of the electron states at the Fermi energy level E_F with increasing OH content could be explained by the N(E_F) of the uniformly O-/OH-/F-terminated surface. Upon full termination of uniform OH species, we observe that the N(E_F) is almost twice as large compared to that of the full O/F termination. Thus, the OH-rich surface should resemble a surface closer to that of the uniformly OH-terminated surface, resulting in an increase in N(E_F). The change in N(E_F) indicates the tunable electronic conductivity of $Ti_3C_2T_x$ via varying the OH/O adatom concentrations on the surface. Higher electronic conductivity, in principle, could potentially be achieved with higher OH concentration.

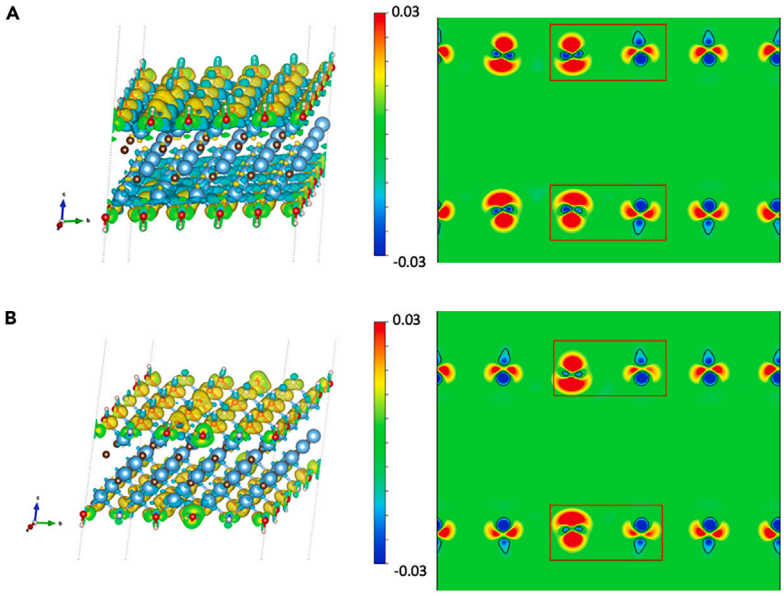

(A) Ordered termination surface of $Ti_3C_2O_{0.24}(OH)_{1.28}F_{0.48}$.
(B) Random termination surfaces of $Ti_3C_2O_{0.24}(OH)_{1.28}F_{0.48}$.
The cyan and yellow regions represent charge depletion and charge accumulation, respectively. Inset shows the 2D slice of the charge density difference viewed from (100) plane with the isovalue ranging from -0.03 to 0.03 e/ Å^3. The region framed in red in the inset indicates a local-induced dipole on the surface.

Figure 3. Charge density difference of $Ti_3C_2O_{0.24}(OH)_{1.28}F_{0.48}$

(A) Ordered termination surface of $Ti_3C_2O_{0.24}(OH)_{1.28}F_{0.48}$.

(B) Random termination surfaces of $Ti_3C_2O_{0.24}(OH)_{1.28}F_{0.48}$.

The cyan and yellow regions represent charge depletion and charge accumulation, respectively. Inset shows the 2D slice of the charge density difference viewed from (100) plane with the isovalue ranging from −0.03 to 0.03 e/Å^3. The region framed in red in the inset indicates a local-induced dipole on the surface.

Charge density difference and electron localization function (ELF)

To further study the charge distribution and the electronic properties of different surface terminations, charge density difference and electron localization function (ELF) calculations were performed. A charge density difference plot was constructed by taking the difference in electron density between the $Ti_3C_2T_x$, pristine Ti_3C_2, and the adatoms to identify the local charge accumulation at the terminated sites. The ELF is often employed to describe and visualize the chemical bonding in molecules or solids[22] and is bound between 0 and 1, where ELF = 1 indicates perfect localization and ELF = 0.5 corresponds to uniform electron gas.

Figure 3 shows the charge density difference of $Ti_3C_2O_{0.24}(OH)_{1.28}F_{0.48}$ with an ordered and random surface distribution. In both cases, charge depletion and accumulation tend to happen at the surface adatoms. Large inhomogeneity of charge depletion/accumulation (ranging from ∼-0.1 e/Å^3 to ∼+0.1 e/Å^3) was observed, as expected, particularly for OH adatom, due to the high polarity of the hydroxyl group. Overall, the dominant charge depletion region is localized at the hydrogen of the hydroxyl group, whereas the charge accumulation is distributed around the electronegative O and F sites of adatoms. Interestingly, from the charge density difference analysis, the electron accumulation/depletion regions are found to be similar among different surface distributions for the termination O/OH/F adatoms (Figure 3). Therefore, the difference in the local distribution of the functional adatoms (i.e., ordered vs. random) does not contribute significantly to the charge density difference. The plot of ELF in Figure 4 gives further insight into the local bonding nature of $Ti_3C_2T_x$. Similar to the charge density difference distribution, the ELF is very similar to both the ordered and random termination. In contrast to this intriguing similarity, the spatial distribution of electrons in the ELF plot is highly localized at the hydroxyl group (ELF ≈ 1), particularly at the H atoms (Figure 4), but not at the O or F adatoms. This is an intriguing observation since the electron localization at the hydroxyl group, regardless of whether the termination is ordered or random, could give rise to the local imbalance surface charge distribution relative to O and F adatoms on $Ti_3C_2T_x$ surfaces as favorable reaction sites, as also indicated by the charge density difference analysis (Figure 3). As a result, this will generate unique locally induced dipoles on the $Ti_3C_2T_x$ surfaces (Figure 3), which might yield important applications in surface chemistry (e.g., gas adsorption and catalysis) as favorable reaction sites on the functionalized $Ti_3C_2T_x$ surface.

Work function

The effects of the surface distribution of different termination groups on the work function for $Ti_3C_2T_x$ were also studied. The work function, Φ, was calculated by computing the planar average of the electrostatic potential along the surface normal direction, as: $\Phi = eV_{vacuum}-E_{Fermi}$,

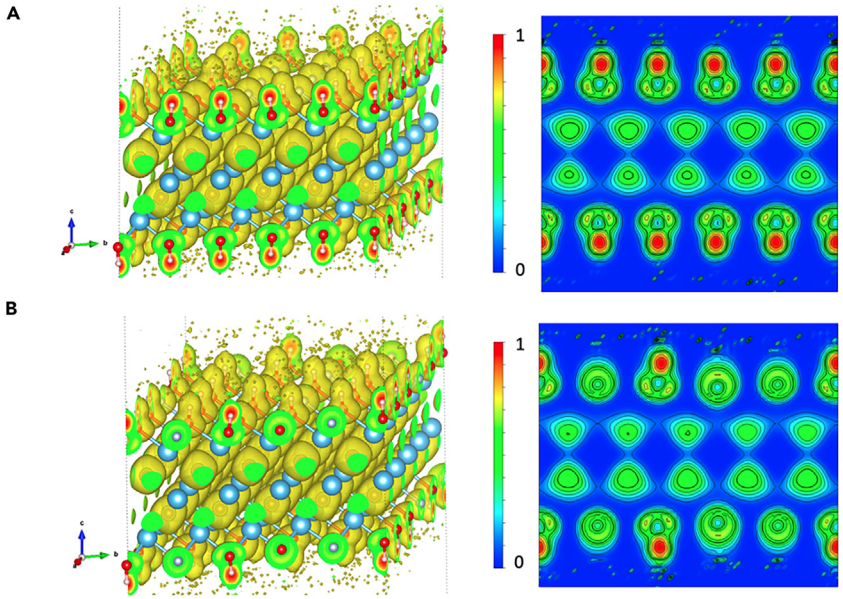

(A) Ordered termination surface of $Ti_3C_2O_{0.24}(OH)_{1.28}F_{0.48}$.
(B) Random termination surfaces of $Ti_3C_2O_{0.24}(OH)_{1.28}F_{0.48}$.
The right panel shows a 2D slice of ELF viewed from the (100) plane. Red and blue regions in the right panel represent localized and delocalized charge with an isovalue of 1 and 0 respectively.

Figure 4. Plot of electron localization function (ELF) of $Ti_3C_2O_{0.24}(OH)_{1.28}F_{0.48}$

(A) Ordered termination surface of $Ti_3C_2O_{0.24}(OH)_{1.28}F_{0.48}$.

(B) Random termination surfaces of $Ti_3C_2O_{0.24}(OH)_{1.28}F_{0.48}$.

The right panel shows a 2D slice of ELF viewed from the (100) plane. Red and blue regions in the right panel represent localized and delocalized charge with an isovalue of 1 and 0, respectively.

where V_{vacuum} is the vacuum potential and E_{Fermi} is the Fermi level. Regardless of the HF concentration, there was an increasing trend in the work function with increasing O concentration.

Among all mixed terminated structures, the minimum work function corresponds to the structures with the most OH content for each HF concentration. As expected, as the acidic environment (or HF concentration) increases, the work functions of $Ti_3C_2T_x$ become gradually higher due to the increase in terminated F content. All the calculated work functions are within the upper (6.04 eV with full O termination) and lower limit (1.81 eV with full OH termination) of the uniformly terminated (O, OH, and F) surfaces. With fixed F percentage coverage on surface termination, a high work function of $Ti_3C_2T_x$ is tunable by decreasing OH termination and increasing O termination. As shown in Figure 5, a linear dependence of the work function with respect to O/OH content is found with the varying stoichiometry. This observed trend is consistent with the reported literature.[18,20]

Despite having different types of surface distributions, no noticeable difference is seen in the work function between the ordered and randomly terminated surfaces, analogous to their relative thermodynamic stability (Table 1). Hence, the work function is, in fact, a function of stoichiometry and is insensitive to the surface termination distribution. Thus, it is possible to experimentally estimate the OH/O composition of $Ti_3C_2T_x$ by measuring the work function. Likewise, the work function can be tuned to the desired value by etching with the appropriate HF concentration. The large tunability in work function for $Ti_3C_2T_x$ (i.e., $\Delta\Phi \sim 3.5$ eV) due to different wt. % of HF (Figure 5) suggests that $Ti_3C_2T_x$ can be strategically modified to suit future electronic device application needs.

Conclusion

A systematic analysis was carried out to determine the effects of varying HF etching concentrations on the thermodynamic stability, electronic properties, and work function of $Ti_3C_2T_x$ based on DFT calculations. Regardless of the HF concentration, surfaces with a larger fraction of OH termination were found to be thermodynamically stable. In addition, the ordered and randomly terminated $Ti_3C_2T_x$ structures are degenerate in their thermodynamic stability, but subtle differences arise from the local clustering of the O functional group, which is found to be less favorable for all cases. Overall, a mixed termination of $Ti_3C_2T_x$ does not alter the metallic nature of Ti_3C_2 but the electronic conductivity varies significantly with OH termination concentration and could be potentially enhanced by increasing its content. In terms of bonding analysis, the charge density difference and ELF demonstrated a significant electron localization at the hydroxyl group, which could yield a locally induced dipole on the surface that could render unique surface chemistry. From DFT predictions, a large tunability in work function for $Ti_3C_2T_x$ (i.e., $\Delta\Phi \sim 3.5$ eV) due to different HF wt. % is found.

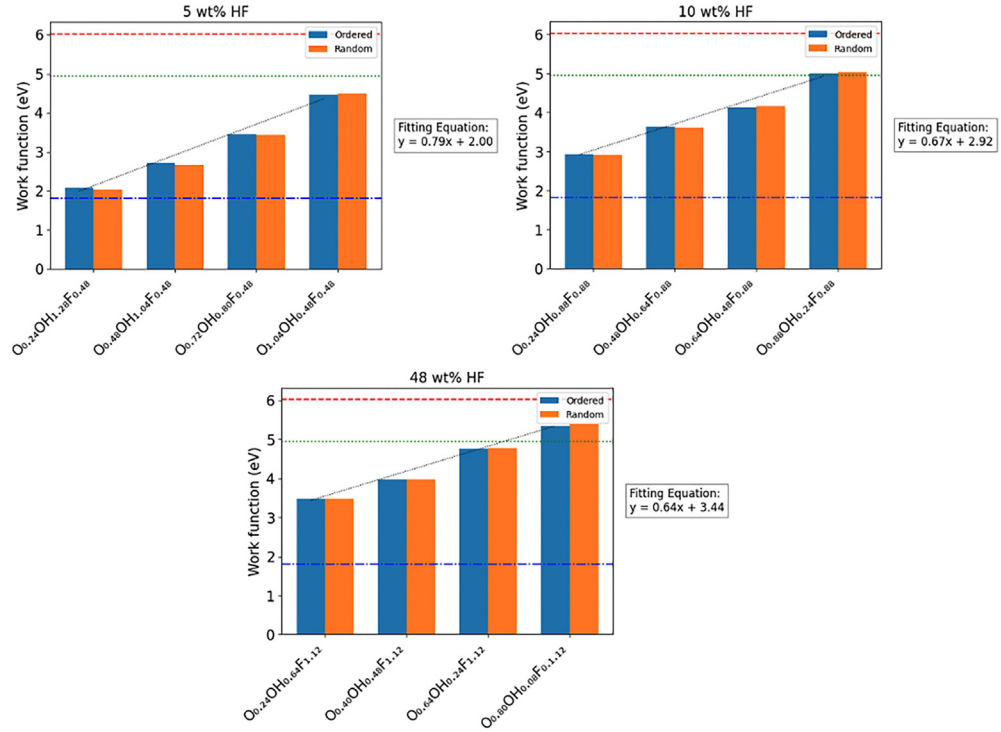

Figure 5. Work function of the $Ti_3C_2T_x$ etched with different HF concentrations

The reference lines correspond to the calculated work function of the uniformly terminated surface. Color code: red: O-termination (6.03 eV), green: F-termination (4.95 eV), blue: OH-termination (1.81 eV).

The work function was found to be a function of the O/OH/F stoichiometry of $Ti_3C_2T_x$ and is independent of the distribution of surface terminations group. For all mixed terminated structures, the minimum work function corresponds to the structures with the most OH content for each HF concentration. As the acidic environment (or HF concentration) increases, the work functions of $Ti_3C_2T_x$ become higher due to the increase in terminated F content. For fixed F content on surface termination, high work function of $Ti_3C_2T_x$ is tunable by decreasing in OH termination and increasing in O termination. The authors believe this work provides valuable insight into the fundamental characterization of $Ti_3C_2T_x$ and a useful design pathway to tune the material properties experimentally through the variation of HF concentration during MAX phase etching to produce the $Ti_3C_2T_x$ MXene.

STAR★METHODS

Detailed methods are provided in the online version of this paper and include the following:

- KEY RESOURCES TABLE
- RESOURCE AVAILABILITY
  - Lead contact
  - Materials availability
  - Data and code availability
- METHOD DETAILS

SUPPLEMENTAL INFORMATION

Supplemental information can be found online at https://doi.org/10.1016/j.isci.2024.108784.

ACKNOWLEDGMENTS

The contribution of computing resources Potassium (through NSF-MRI: NSF OAC-2117956) and Nature HPC cluster at California State University, Northridge is acknowledged. This material is based upon work supported by the US Department of Energy, Office of Science, Office of

Basic Energy Sciences, Division of Materials Sciences and Engineering We would also like to thank our technical editor, Kent Cubbage, for proofreading the manuscript before submission.

AUTHOR CONTRIBUTIONS

Y.Z.C. and M.H. conducted the calculations and simulations. K.C.L designed the workflow and study. P.W. and K.C.L. secured funding and provided mentoring. Y.Z.C. wrote the manuscript. M.H., K.C.L., and P.W. revised the manuscript.

DECLARATION OF INTERESTS

The authors declare no competing interests.

Received: July 20, 2023
Revised: August 30, 2023
Accepted: January 2, 2024
Published: January 4, 2024

REFERENCES

1. Novoselov, K.S., Geim, A.K., Morozov, S.V., Jiang, D., Zhang, Y., Dubonos, S.V., Grigorieva, I.V., and Firsov, A.A. (2004). Electric Field Effect in Atomically Thin Carbon Films. Science *306*, 666–669.
2. Gogotsi, Y., and Anasori, B. (2019). The Rise of MXenes. ACS Nano *13*, 8491–8494.
3. Yorulmaz, U., Demiroğlu, İ., Çakir, D., Gülseren, O., and Sevik, C. (2020). A systematical ab-initio review of promising 2D MXene monolayers towards Li-ion battery applications. JPhys Energy *2*, 032006.
4. Xie, Y., Naguib, M., Mochalin, V.N., Barsoum, M.W., Gogotsi, Y., Yu, X., Nam, K.-W., Yang, X.-Q., Kolesnikov, A.I., and Kent, P.R.C. (2014). Role of Surface Structure on Li-Ion Energy Storage Capacity of Two-Dimensional Transition-Metal Carbides. J. Am. Chem. Soc. *136*, 6385–6394.
5. Lee, E., and Kim, D.-J. (2020). Review—Recent Exploration of Two-Dimensional MXenes for Gas Sensing: From a Theoretical to an Experimental View. J. Electrochem. Soc. *167*, 037515.
6. Hu, Q., Sun, D., Wu, Q., Wang, H., Wang, L., Liu, B., Zhou, A., and He, J. (2013). MXene: A New Family of Promising Hydrogen Storage Medium. J. Phys. Chem. A *117*, 14253–14260.
7. Khazaei, M., Arai, M., Sasaki, T., Chung, C.-Y., Venkataramanan, N.S., Estili, M., Sakka, Y., and Kawazoe, Y. (2013). Novel Electronic and Magnetic Properties of Two-Dimensional Transition Metal Carbides and Nitrides. Adv. Funct. Mater. *23*, 2185–2192.
8. Naguib, M., Kurtoglu, M., Presser, V., Lu, J., Niu, J., Heon, M., Hultman, L., Gogotsi, Y., and Barsoum, M.W. (2011). Two-Dimensional Nanocrystals Produced by Exfoliation of Ti3AlC2. Adv. Mater. *23*, 4248–4253.
9. Wang, X., Shen, X., Gao, Y., Wang, Z., Yu, R., and Chen, L. (2015). Atomic-Scale Recognition of Surface Structure and Intercalation Mechanism of Ti3C2X. J. Am. Chem. Soc. *137*, 2715–2721.
10. Er, D., Li, J., Naguib, M., Gogotsi, Y., and Shenoy, V.B. (2014). Ti3C2 MXene as a High Capacity Electrode Material for Metal (Li, Na, K, Ca) Ion Batteries. ACS Appl. Mater. Interfaces *6*, 11173–11179.
11. Shein, I.R., and Ivanovskii, A.L. (2012). Graphene-like titanium carbides and nitrides Tin+1Cn, Tin+1Nn (n=1, 2, and 3) from de-intercalated MAX phases: First-principles probing of their structural, electronic properties and relative stability. Comput. Mater. Sci. *65*, 104–114.
12. Cheng, Y., Ma, X., Huang, C., Yuan, G., and Liao, J. (2022). The effect of functional groups (O, F, or OH) on reversible hydrogen storage properties of Ti2X (X=C or N) monolayer. Int. J. Hydrogen Energy *47*, 28969–28977.
13. Schultz, T., Frey, N.C., Hantanasirisakul, K., Park, S., May, S.J., Shenoy, V.B., Gogotsi, Y., and Koch, N. (2019). Surface Termination Dependent Work Function and Electronic Properties of Ti3C2Tx MXene. Chem. Mater. *31*, 6590–6597.
14. Li, H., Li, A., Zhang, D., Wu, Q., Mao, P., Qiu, Y., Zhao, Z., Yu, P., Su, X., and Bai, M. (2022). First-Principles Study on the Structural, Electronic, and Lithium Storage Properties of Ti3C2T2 (T = O, F, H, OH) MXene. ACS Omega *7*, 40578–40585.
15. Wang, H.-W., Naguib, M., Page, K., Wesolowski, D.J., and Gogotsi, Y. (2016). Resolving the Structure of Ti3C2Tx MXenes through Multilevel Structural Modeling of the Atomic Pair Distribution Function. Chem. Mater. *28*, 349–359.
16. Karlsson, L.H., Birch, J., Halim, J., Barsoum, M.W., and Persson, P.O.Å. (2015). Atomically Resolved Structural and Chemical Investigation of Single MXene Sheets. Nano Lett. *15*, 4955–4960.
17. Shi, C., Beidaghi, M., Naguib, M., Mashtalir, O., Gogotsi, Y., and Billinge, S.J.L. (2014). Structure of Nanocrystalline Ti3C2 MXene Using Atomic Pair Distribution Function. Phys. Rev. Lett. *112*, 125501.
18. Caffrey, N.M. (2018). Effect of mixed surface terminations on the structural and electrochemical properties of two-dimensional Ti3C2T2 and V2CT2 MXenes multilayers. Nanoscale *10*, 13520–13530.
19. Ibragimova, R., Erhart, P., Rinke, P., and Komsa, H.-P. (2021). Surface Functionalization of 2D MXenes: Trends in Distribution, Composition, and Electronic Properties. J. Phys. Chem. Lett. *12*, 2377–2384.
20. Ibragimova, R., Puska, M.J., and Komsa, H.-P. (2019). pH-Dependent Distribution of Functional Groups on Titanium-Based MXenes. ACS Nano *13*, 9171–9181.
21. Wang, S., Liu, Y., Liu, Y., Shi, Z., Zhou, J., Zhu, J., and Hu, W. (2022). Identifying the surface properties of Ti3C2Tx MXene through transmission electron microscopy. Cell Reports Physical Science *3*, 101151.
22. Kohout, M., Wagner, F.R., and Grin, Y. (2002). Electron localization function for transition-metal compounds. Theor. Chem. Acc. *108*, 150–156.
23. Kresse, G., and Furthmüller, J. (1996). Efficiency of ab-initio total energy calculations for metals and semiconductors using a plane-wave basis set. Comput. Mater. Sci. *6*, 15–50.
24. Kresse, G., and Furthmüller, J. (1996). Efficient iterative schemes for ab initio total-energy calculations using a plane-wave basis set. Phys. Rev. B *54*, 11169–11186.
25. Perdew, J.P., Burke, K., and Ernzerhof, M. (1996). Generalized Gradient Approximation Made Simple. Phys. Rev. Lett. *77*, 3865–3868.
26. Grimme, S. (2006). Semiempirical GGA-type density functional constructed with a long-range dispersion correction. J. Comput. Chem. *27*, 1787–1799.
27. Momma, K., and Izumi, F. (2011). VESTA 3 for three-dimensional visualization of crystal, volumetric and morphology data. J. Appl. Crystallogr. *44*, 1272–1276.
28. Almeida, M.O., Kolb, M.J., Lanza, M.R.V., Illas, F., and Calle-Vallejo, F. (2022). Gas-Phase Errors Affect DFT-Based Electrocatalysis Models of Oxygen Reduction to Hydrogen Peroxide. Chemelectrochem *9*, e202200210.
29. Sargeant, E., Illas, F., Rodríguez, P., and Calle-Vallejo, F. (2021). Importance of the gas-phase error correction for O2 when using DFT to model the oxygen reduction and evolution reactions. J. Electroanal. Chem. *896*, 115178.
30. Granda-Marulanda, L.P., Rendón-Calle, A., Builes, S., Illas, F., Koper, M.T.M., and Calle-Vallejo, F. (2020). A Semiempirical Method to Detect and Correct DFT-Based Gas-Phase Errors and Its Application in Electrocatalysis. ACS Catal. *10*, 6900–6907.

STAR★METHODS

KEY RESOURCES TABLE

REAGENT or RESOURCE	SOURCE	IDENTIFIER
Software and algorithms		
VASP	VASP Software GmbH	https://www.vasp.at/
VESTA software package	JP-Minerals	https://jp-minerals.org/vesta/en/

RESOURCE AVAILABILITY

Lead contact

Further information and requests for resources should be directed to the lead contact, Kah Chun Lau (kahchun.lau@csun.edu).

Materials availability

This study did not yield new unique reagents.

Data and code availability

- The simulation data that support the findings of this study are available from the lead contact upon reasonable request.
- This paper does not report original code.
- Any additional information required to analyze the data reported in this paper is available from the lead contact upon reasonable request.

METHOD DETAILS

To model the 2D $Ti_3C_2T_x$ structures, first-principles DFT was employed as implemented in Vienna Ab initio Simulation Package (VASP)[23,24] for the spin-polarized electronic structure calculations. The projector-augmented-wave (PAW) pseudopotential method, together with the generalized gradient approximation and the Perdew–Burke–Ernzerhof (PBE) exchange-correlation functional were used to represent the exchange-correlation effects in the DFT simulation.[25] The kinetic energy cutoff for the plane-wave basis was set at 500 eV. For the structural optimization and electronic calculations, the Brillouin zone was sampled using a Γ-centered grid of (3 × 3×1) where the convergence in the total energy (<0.02 eV) is achieved with respect to the number of k points, while the eDOS (DOS) was sampled using a grid of (9 × 9×1). The electronic self-consistent cycle energy convergence was set at $1\times10^{-5}eV$ and the residual force on each atom is less than $1 \times 10^{-4}eV/$ Å. The van der Waals interaction was included in all calculations using the semi-empirical approach of Grimme (DFT-D3).[26] For the monolayer structure calculations, a vacuum slab of at least 15 Å along the z axis was implemented to avoid interactions between mirror images. To further confirm the thermal stability of these $Ti_3C_2T_x$ (Table 1) at room temperature, ab initio molecular dynamics was performed on two selected structures for 10 ps in the NVT ensemble employing Nosé–Hoover thermostats, and the results are shown in Figure S11. Our result shows no significant structure deformation or dissociation of termination groups upon heating at T = 300 K, confirming the thermal stability of our structures at room temperature. All atomic structures and charge densities are visualized using VESTA.[27]

To compute the formation energy of various mixed terminated $Ti_3C_2T_x$ structures with different local site distribution (i.e., ordered vs. random) of O/OH/F adatoms (Table 1), the reference energies of the adatoms are computed by considering the total energy and thermal energy corrections of a single molecule for OH and one-half of the total energy of O_2 and F_2 for O and F, respectively. In gas-phase calculations that employ DFT-GGA, the overestimation of the binding energy often arises due to the limitations in describing the exchange energy of first-row elements, such as molecular oxygen.[28,29] To overcome these effects, one could add an empirical correction to the DFT energy[30] or use a more accurate, albeit computationally expensive, hybrid or *meta*-GGA functional. In this study, we were interested in the qualitative difference between the adatom adsorptions, thus, an empirical correction was not included. Since the calculated formation energies depend on the employed thermodynamic equations, to further justify the predicted formation energy of mixed terminated $Ti_3C_2T_x$ structures highlighted in Table 1, another set of reference energies of the O/OH/F adatoms by considering the splitting of H_2O and HF proposed from ref. 19,20 is adopted (Table S1). Despite using different reference energies of O/OH/F adatoms, some common trends can be found in Tables 1 and S1. As indicated in Tables 1 and S1, both the ordered and random distribution of O/OH/F adatoms on mixed terminated $Ti_3C_2T_x$ surfaces exhibit nearly similar thermodynamic stability, regardless of different HF wt %. Interestingly in both cases (*i.e.*, Tables 1 and S1), OH-rich surfaces are generally found to be thermodynamically stable in different HF concentrations, and therefore one can conclude that the presence of OH-rich surfaces at various mixed terminated $Ti_3C_2T_x$ is highly plausible. For conciseness, we only considered the thermodynamic stability referring to Table 1 in our discussion. The surface distributions presented here (Tables 1 and S1) are the representative cases with the lowest energy among 2–3 different models per distribution (i.e., ordered and random) for each stoichiometry.